Bull. Chem. Soc. Ethiop. **2023**, 37(1), 171-181.
DOI:https://dx.doi.org/10.4314/bcse.v37i1.14
© 2023 Chemical Society of Ethiopia and The Authors
ISSN 1011-3924
Printed in Ethiopia
Online ISSN 1726-801X

BENZOIC ACID DERIVATIVES: ANTI-BIOFILM ACTIVITY IN *PSEUDOMONAS AERUGINOSA* PAO1, QUANTUM CHEMICAL CALCULATIONS BY DFT AND MOLECULAR DOCKING STUDY

Neslihan Kaya Kınaytürk[1], Ebru Önem[2] and Halil Oturak[3]

[1]Department of Nanoscience and Nanotechnology, Faculty of Arts and Sciences, Burdur Mehmet Akif Ersoy University, Burdur, Turkey
[2]Faculty of Pharmacy, Suleyman Demirel University, Isparta, Turkey
[3]Department of Physics, Faculty of Arts and Sciences, Süleyman Demirel University, Isparta, Turkey

(Received April 18, 2022; Revised August 9, 2022; Accepted August 9, 2022)

ABSTRACT. Quorum sensing (QS), used by many pathogenic bacteria to express virulence factors, is seen as a new and effective strategy to combat resistant bacteria. In this study, theoretical investigations were made on the structural data of molecules to support the inhibition effects of 2-amino 4-chloro benzoic acid and 4-amino 2-chloro benzoic acid molecules. Theoretical calculations were performed by using the density functional theory with the B3LYP function and aug-cc-pVDZ basis set in the gas phase of the isolated compounds in the ground state. The biological activities of the related compounds were theoretically investigated against Covid-19 protein (PDB ID: 6LU7).

KEY WORDS: 2-Amino-4-chlorobenzoic acid, 4-Amino-2-chlorobenzoic acid, Quorum sensing, Molecular docking

INTRODUCTION

Benzoic acid, the simplest aromatic carboxylic acid, is frequently used in areas such as food, personal care products, and the pharmaceutical industry [1]. While ointments containing benzoic acid are used in the treatment of fungal diseases because they prevent the formation of yeast and bacteria, they are also used as anticancer and influenza neuraminidase inhibitors due to their antifungal and antibacterial properties [2, 3]. In the literature, it is possible to come across many studies on benzoic acid derivatives in the field of pharmacology from past to present [4]. It is stated in the literature that the reason why benzoic acid derivatives are frequently preferred in the field of pharmacology is due to their nucleophilic and electrophilic properties in the structure of their molecules [5]. In recent years, the examination of benzoic acid derived compounds in the treatment of Covid-19, as well as cancer treatment, is quite remarkable [2, 5-7].

Pseudomonas aeruginosa is an opportunistic human pathogen, especially responsible for chronic lung diseases in patients with cystic fibrosis [8]. *P. aeruginosa* infection develops in three stages: colonization, invasion and systemic spread. The pathogenicity is defined as pathogenicity when the microorganism reproduces in the host and performs the steps mentioned above, and the structures responsible for pathogenicity are called virulence factors. This step called quorum sensing (QS) and is an intercellular signaling pathway can be expressed as gene coordination depending on the population density of bacteria [9] *P. aeruginosa* produces many virulence factors such as elastase, pyocyanin, protease production, swarming motility and biofilm formation thanks to this system [10]. Biofilms that can form on medical devices and biomaterials as well as on host epithelial cells and mucosal surfaces play a role in many different diseases such as chronic wound infections, cystic fibrosis, endocarditis [11-13]. The mechanical and physicochemical properties of biofilm matrix prevent the penetration of many compounds, including antibiotics

*Corresponding author. E-mail: nkinayturk@mehmetakif.edu.tr
This work is licensed under the Creative Commons Attribution 4.0 International License

and antiseptics, to reach the bacterial cell within the biofilm. The inhibition of the QS system, which is important in biofilm formation, is becoming increasingly important [14]. Up to now, many natural and synthetic molecules have been tried on the inhibition of the system. Some of these are AHL analogues, furanone derivatives, plant extracts, different heterocyclic molecules and many known drug active ingredients [15].

Nowadays, theoretical calculations are known as a good guide for experimental studies. Therefore, theoretical calculations are often used to compare the chemical and biological activities of molecules [16]. With the DFT method, it is possible to reach clear information about the charge transfer within the molecule.

In our previous study, the spectroscopic properties (conformer, vibration, NMR and UV-Vis analyses) of 2-amino 4-chlorobenzoic acid (2A4ClBA) and 4-amino 2-chlorobenzoic acid (4A2ClBA) molecules were elucidated [17]. This study was planned as a complement to our previous study. In this study, it was aimed to elucidate the optical and electronic structures of 2A4ClBA and 4A2ClBA molecules, to investigate their inhibition effects on biofilm formation on PAO11, and also to examine their interactions with Covid-19 proteins.

EXPERIMENTAL

Biofilm assay

Anti-biofilm effect of molecules tested by cristal violet (CV) assay [14]. *P. aeruginosa* PAO1 was grown in 200 µL LB broth medium with test compounds (final concentration 2 and 3 mM) and incubated 37 °C for 48 h. Following 48 hours incubation at 37 °C, the microplates were washed with distilled water 3-5 times to remove the planktonic bacteria. The resting bacteria dyed with 0.1% crystal violet. After about 30 min. wells washed again distilled water. Ethanol was added to the wells to dissolve the stained biofilm layer. At the end of 15 min the absorbance was measured at 570 nm (Biotek-Epoch 2 Microplate Spectrophotometer, Winooski, Vermont USA).

Computational details

Gaussian 09 [18] software package was used for the theoretical calculations. The DFT method resolves both the energy of a molecule for its electron density and describes it without evaluating it from the total wave function. For quantum chemical calculations, results were obtained using the density functional theory (DFT) method with the B3LYP functional and aug-cc-pVDZ basis set. Time-dependent DFT (TD-DFT) method was used to obtain electronic properties. The results were visualized using the Gauss View program [19]. Molecular docking study was investigated using the program Autodock Vina [20].

Statistical evaluation

Data were subjected to analysis of variance (ANOVA) with JUMP software and the differences were compared by LSD test.

RESULTS AND DISCUSSION

Inhibition of virulence factors

In the present study bacterial biofilm inhibition of benzoic acid derivatives were investigated different concentration in *P. aeruginosa* PAO1. In the biofilm form, bacteria are more resistant to antimicrobial treatments. Bacteria in a biofilm can also survive in adverse conditions and protect itself from the host's immune system [21]. Therefore, preventing biofilm formation is of great

importance in combating infectious diseases. The discovery of the QS has been seen as a promising approach to combating bacteria and has been the focus of studies. Besides plants, many existing and newly synthesized synthetic molecules have been tried for the inhibition of the system. This study focused on the inhibitory effect of two benzoic acid derivatives on biofilm formation in PAO1. 2A4ClBA and 4A2ClBA molecules were used in tests at 2 mM and 3 mM concentrations that do not inhibition effect of bacterial growth. According to results the most inhibition effect was detected 3 mM concentration of 2A4ClBA molecule by 67% and 4A2ClBA molecules showed moderate inhibition both concentration by 28%, 24%, respectively. All results were statistically significant when compared to control PAO1 ($p < 0.01$) (Figure 1).

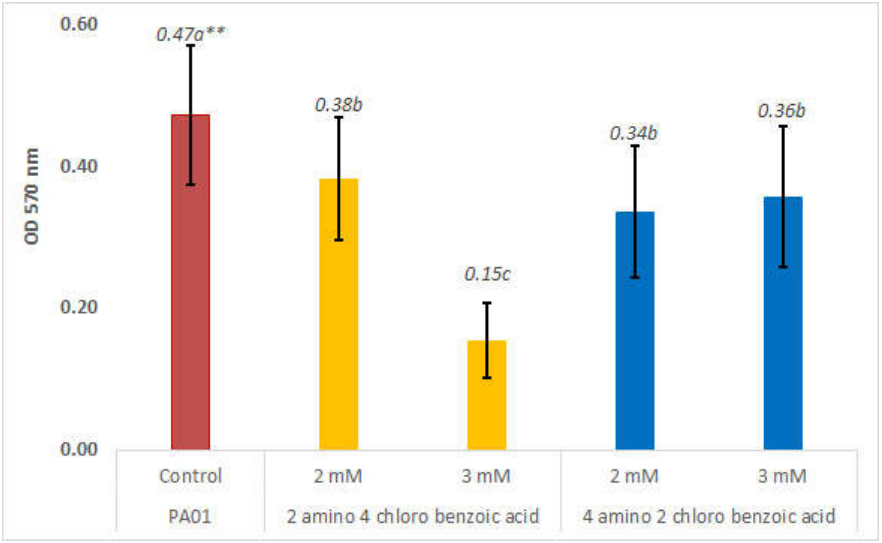

Figure 1. Inhibition effect of 2A4ClBA and 4A2ClBA molecules on biofilm formation. **Differences between mean values followed by different letters of molecules statistically significant at $p < 0.01$.

Molecular electrostatic potential surface (MEP) and Mulliken charge distribution

Molecular electrostatic potential surface maps (MEP) provide information about the charge distribution as well as observing the variable charge regions of molecules [22]. Charge distribution is a method often used to predict intermolecular interactions, molecular behavior, structural activity, electrophilic and nucleophilic reactivity, as well as detailing hydrogen bonding [23]. Figure 2 presents a color-coded picture of the electrostatic potential surface. In the MEP map, the electron-deficient region is coded in blue, the electron-rich region is coded in red, and the neutral, zero electrostatic potential region showing hydrogen-bond interactions is coded in green [24]. For 2A4ClBA, scaling order ranges from –1.63 eV (red) strongest attraction to 1.63 eV (blue) strongest repulsion. Similarly, the scaling order for the 4A2ClBA molecule ranges from -1.62 eV (red) strongest attraction to 1.62 eV (blue) strongest repulsion. The MEP map shows that the negative potential regions are on the oxygen atoms, hence these show the most favored site for any electrophilic attack on the molecules. The maximum positive regions are localized on the H atoms in the carbonyl and amine groups, indicating a possible site for nucleophilic attack.

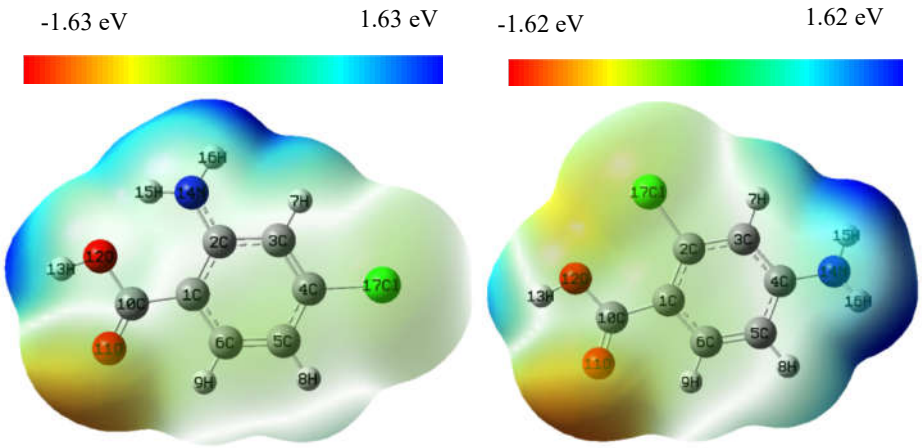

Figure 2. Molecular electrostatic potential surface map calculated for (a) 2A4ClBA and (b) 4A2ClBA.

The atomic charge of a molecule is a fundamental chemical property. It is preferred to explain the charge transfer mechanism and electronic structures in chemical reactivities [24]. The results of Mulliken population analysis (MPA) are used to explain the differences in electronegativity of atoms in the molecule and to interpret and predict electrophilic and nucleophilic reagent behavior. Therefore, calculation of atomic charges plays an important role in DFT studies of molecular systems. In addition, the atomic charge is a factor that affects the dipole moment, polarizability, electronic structure, and other molecular properties of the system [2]. Mulliken charges of the title molecules were calculated on the B3LYP/aug-cc-pVDZ basis set and the details are presented in Figure 3. The DFT calculation showed that the oxygen atoms of the optimized compounds have negative charge acting as donor atoms. Mulliken charges of O11 and O12 atoms for 2A4ClBA and 4A2ClBA molecules were calculated as -0.556637, -0.547055 a.u. and -0.606569, -0.576324, a.u., respectively. It is important to note that for title molecules, unlike other hydrogen atoms, the H13 atom acquires a positive charge due to the presence of the electronegative O12 atom. C2 in the benzene ring attached to the N14 atom of 2A4ClBA and C4 in the benzene ring attached to the N14 atom of 4A2ClBA have negative charges of -0.832408 and -0.926451 a.u., respectively.

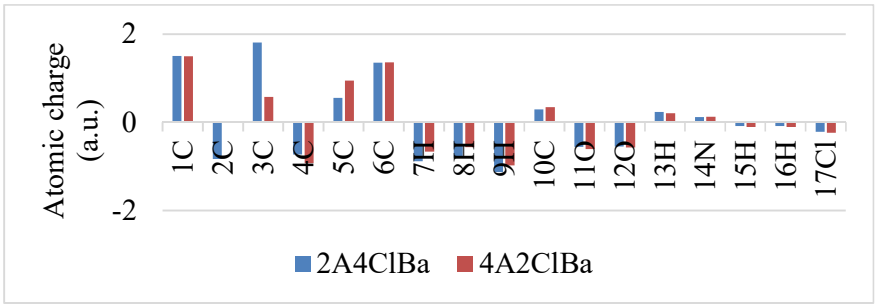

Figure 3. Atomic charge distribution of 2A4ClBA and 4A2ClBA.

Frontier molecular orbitals (FMOs) and chemical activity

The ability of a molecule to donate and accept electrons is defined using the HOMO and LUMO energy values. They are called frontier molecular orbitals (FMOs) because they are located at the outermost frontier of the electrons of the molecules [25]. While FMO plays an important role in molecular orbitals, electronic and optical properties, UV-VIS, quantum chemistry, luminescence, photochemical reaction, and pharmaceutical studies, it allows us to learn about biological mechanisms [26]. The energy difference between HOMO and LUMO gives important information about the chemical stability of a molecule. Large HOMO-LUMO energy differences indicate less polarizability, high kinetic stability, and low chemical reactivity [27]. Molecules with a large energy gap are more stable than molecules with a small energy gap. The HOMO-LUMO gap also describes the intramolecular charge transfer in a molecule [28]. The HOMO and LUMO surface images are given in Figure 3 and the calculated parameters are given in Table 1. The HOMO and LUMO energies of 2A4ClBA and 4A2ClBA molecules was calculated -6.214; -1.82 and -6.35; -1.64 eV, respectively. Therefore, the band gaps were calculated as 4.37 and 4.71 eV, respectively. A negative chemical potential (μ) value indicates the stability of a molecule and means that the molecule will not easily decompose into its elements. Hardness (n) is defined as the character of molecules that resist deforming the molecular electron cloud under minor perturbations. A hard molecule has a large HOMO-LUMO band gap. Thus, the molecule has low polarization, chemical and biological activity, but high kinetic sensitivity. On the other hand, a soft molecule, has a small HOMO-LUMO energy difference. It has high polarizability, chemical and biological activities but low kinetic sensitivity of the molecule. Hard molecules are considered to be less reactive than soft molecules. The electrophilicity index is used to obtain information about the structure, toxicity, reactivity, and dynamics of a molecule. Organic molecules with an electrophilic (ω) index value > 1.5 eV can be defined as strong electrophiles. The w value for 2A4ClBA and 4A2ClBA molecules was calculated as 3.672 and 3.389 eV, respectively, so we can say that both molecules have electrophilic properties as well as chemical and biological activities. It is also supported by many benzoic acid derivative molecules in the literature that both molecules have high chemical and biological properties [2, 5, 29-31].

Table 1. Global chemical reactivity indices for the 2A4ClBA and 4A2ClBA.

Parameters	2A4ClBA (eV)	4A2ClBA (eV)
E_{HOMO}	-6.21	-6.35
E_{LUMO}	-1.82	-1.64
ΔE	4.37	4.71
Ionization potential ($I = - E_{HOMO}$)	6.21	6.35
Electron affinity ($A = - E_{LUMO}$)	1.82	1.64
Electronegativity ($\chi = (I+A)/2$)	4.015	3.995
Chemical potential ($\mu = -(I+A)/2$)	-4.015	-3.995
Chemical hardness ($\eta = (I-A)/2$)	2.195	2.355
Chemical softness ($s = 1/2\eta$)	0.228	0.212
Electrophilic index ($w = \mu^2/2\ \eta$)	3.672	3.389
Maximum load transfer parameter ($\Delta N_{max} = (I+A)/2(I-A)$)	0.915	0.848

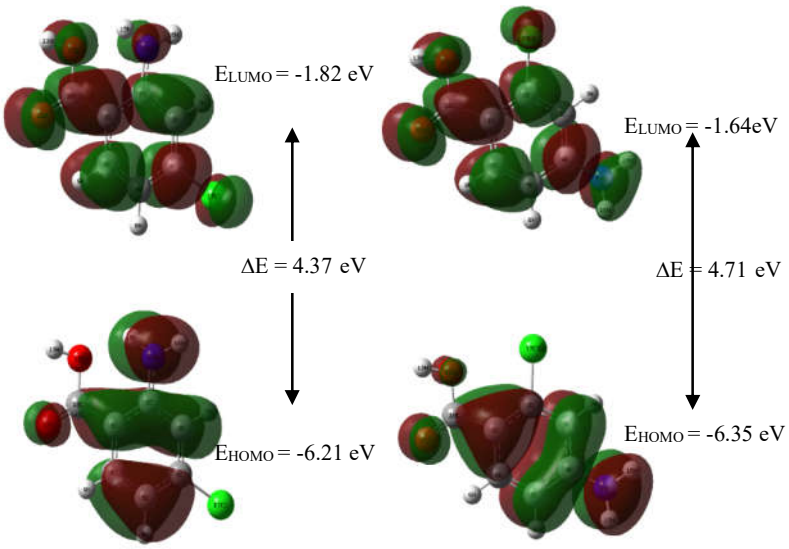

Nonlinear optical properties (NLO)

Figure 4. HOMO and LUMO plot of (a) 2A4ClBA (b) 4A2ClBA.

In the field of optoelectronic applications, the structure and optical properties of the material play a vital role. Polarizability and hyperpolarizability are used as quantitative structure-activity relationship tools as important tools in pharmacology, drug design, and industrial fields. For the title molecules, the dipole moment (μ), the polarizabilities (α), and the first-order hyperpolarizabilities (β) at the static state were computed by using the keyword polar = enonly with the B3LYP/aug-cc-pVDZ level. The quantities of μ, α and β in terms of x, y, and z components are listed in Table 2. The μ_{total}, <α> and β_{total} quantities were obtained via the following equations [28];

$$\mu_{total} = \left(\mu_x{}^2 + \mu_y{}^2 + \mu_z{}^2\right)^{\frac{1}{2}} \quad (1)$$

$$\alpha_{total} = \frac{1}{3}\left(\alpha_{xx} + \alpha_{yy} + \alpha_{zz}\right) \quad (2)$$

$$\beta_o = \left[\left(\beta_{xxx} + \beta_{xyy} + \beta_{xzz}\right)^2 + \left(\beta_{yyy} + \beta_{yzz} + \beta_{yxx}\right)^2 + \left(\beta_{zzz} + \beta_{zxx} + \beta_{zyy}\right)^2 \right. \quad (3)$$

These calculated values allow to determine the strength of molecular interactions, as well as the cross-section of different scattering and collision processes. Thus, the computational approach is a good inexpensive guide in designing new molecules by evaluating the potentials of the molecules before synthesis [32]. Polarizability and hyperpolarizability values calculated with Gaussian 09 are reported as atomic units (a.u), the calculated values are converted to electrostatic units (e.s.u.) (For α, 1 a.u. = $0.1482*10^{-24}$ esu, for β, 1 a.u. = $0.008629*10^{-30}$ esu). The hyperpolarizability value of urea is used as a reference for compounds with nonlinear optical properties. In this study, dipole moment (μ), polarizability (<α>) and first-order hyperpolarizability (β) values for urea were calculated as 1.726 D, 5.459 x 10^{-24} esu and 63.355 x 10^{-30} esu, respectively, using the same basis set. The dipole moment (μ), polarizability (α) and

first-order hyperpolarizability (β) values of urea, 2A4ClBA and 4A2ClBA molecules are given in Table 2 in detail. When Table 2 is examined, it is seen that the dipole moment values of 2A4ClBA and 4A2ClBA molecules are almost similar to the dipole moment of urea (1.741 D), which shows strong intermolecular interactions. The polarizability values for 2A4ClBA and 4A2ClBA molecules were calculated as 18.06×10^{-24} and 18.08×10^{-24}, respectively, and when these values were compared with the polarizability value of urea, it was observed that the polarizability values of the title molecules were approximately 3.3 times higher than that of urea. It is also very striking that the first-order hyperpolarizability (β) values of 2A4ClBA and 4A2ClBA are approximately 45 and 95 times greater than that of urea. These results show that 2A4ClBA and 4A2ClBA molecules are very good candidates for nonlinear optical materials.

Yadav *et al.*, in their study on 4-bromo-3-(methoxymethoxy) benzoic acid in 2022, calculated the polarizability value as 2.1880×10^{-23} and the first-order hyperpolarizability (β) value as 9.7419×10^{-30} [29]. In 2019, Santy *et al.* reported the polarizability and the first-order hyperpolarizability (β) values of 2.6 bis (three fluoro methyl) benzoic acid molecules as 2.9591×10^{-23} and 1.0759×10^{-30}, respectively [33]. This literature study supports that the nonlinear optical properties of the title molecules are quite good.

Table 2. Dipole moments, static average polarizability, further extended first hyperpolarizability of 2A4ClBA and 4A2ClBA.

Components	2A4ClBA	4A2ClBA	Urea	Components	2A4ClBA	4A2ClBA	Urea
μ_x	-0.380	1.667	0.00	β_{xxx} (a.u)	-675.478	-978.610	0.0275
μ_y	1.254	0.222	-1.726	β_{xyy}(a.u)	131.449	129.807	30.713
μ_z	0.009	0.263	0.001	β_{xxy}(a.u)	-131.732	-248.924	-0.542
μ_{total} (D)	1.310	1.702	1.726	β_{yyy}(a.u)	-116.569	5.171	93.517
α_{xx} (a.u)	172.182	170.395	41.476	β_{xxz}(a.u)	2.951	14.429	-0.021
α_{xy} (a.u)	-0.883	-0.199	0.00	β_{yyz}(au)	2.027	3.741	-0.803
α_{yy}(a.u)	127.387	129.590	41.771	β_{xzz}(a.u)	16.641	46.868	0.031
α_{xz} (a.u)	0.117	-0.266	-0.001	β_{yzz}(a.u)	7.470	-1.558	-38.551
α_{yz} (a.u)	-0.009	-0.106	0.001	β_{zzz}(a.u)	1.003	3.242	-0.058
α_{zz}(a.u)	65.954	66.047	27.042	β_{total}(esu)	29.01×10^{-28}	60.73×10^{-28}	63.355×10^{-30}
$<\alpha>$ (a.u)	121.841	122.011	36.76				
$<\alpha>$ (esu)	18.06×10^{-24}	18.08×10^{-24}	5.459×10^{-24}				

Molecular docking

The molecular docking method, which has been frequently preferred in rational drug design in recent years, has great importance in elucidating drug-enzyme interactions [34, 35].

In the literature, it has been seen that many benzoic acid derivative complexes are preferred in the synthesis of alternative drugs for the treatment of Covid-19 [5]. Here, we focused on the major prostease of PDB ID: 6LU7, a potential target protein for the treatment of COVID-19 [26, 36-39]. Because some amino acids of the holo form of the main protease of the 6LU7 protein have been noted in many articles to interact with favipiravir. In this study, it was investigated whether an interaction similar to the interaction between 6LU7 protein and favipiravir also occurs with benzoic acid derivatives. Therefore, in this study, a molecular docking study was performed to predict the interactions of the active binding sites of the Covid-19 main prosthesis and the 2A4ClBA and 4A2ClBA molecules from benzoic acid derivatives. The three-dimensional crystal structure of the targeted protein (PDB ID: 6LU7) was obtained from the RSBC PDB format.

The molecular docking method offers many parameters related to the biological activities of molecules. It is possible to obtain information about molecules by comparing the numerical values of these parameters. The most important parameter is the docking score which gives information

about biological activity. The molecule with the most negative numerical value has the highest biological activity value, and high biological activity indicates the highest interaction between proteins and the molecule [2].

Molecular docking was done using Autodock Vina software. Autodock Tool was used to create doking data entry files, and PyMol program were used to demonstrate Receptor-ligand interactions. The Autodock Tool version 1.5.6 package program was used for protein optimization by removing water and other atoms and adding a polar hydrogen group.

According to the AutoDock Vina result, the best binding affinities of 2A4ClBA and 4A2ClBA molecules on the 6LU7 protein were calculated as -6.6 and -6.2 kcal/mol, respectively. Binding affinity values for nine different binding poses are given in Table 3. The interactions between the ligands 2A4ClBA and 4A2ClBA and the 6LU7 protein are shown in Figure 5. For the 2A4ClBA ligand, the interactions between the PHE active residue and the O11 atom of the ligand, between the HIS active residue and the O12 atom, between the TRY active residue and the H8 atom of the ligand, and between the LYS active residue and the H13 atom of the ligand are clearly seen in Figure 5a.

Table 3. The binding affinity values of different poses of the title compound predicted by Autodock Vina.

	2A4ClBA			4A2ClBA		
		Distance from best mode (Å)			Distance from best mode (Å)	
Mode	Affinity (kcal/mol)	RMSD 1.b	RMSD u.b.	Affinity (kcal/mol)	RMSD 1.b	RMSD u.b.
1	-6.6	0.000	0.000	-6.2	0.000	0.000
2	-6.1	15.802	16.717	-5.8	15.379	16.333
3	-6.0	3.611	4.239	-5.8	1.813	2.312
4	-5.9	14.632	15.560	-5.8	14.562	15.488
5	-5.4	3.522	4.345	-5.7	3.526	4.203
6	-5.4	15.874	16.824	-5.5	13.902	14.816
7	-5.4	1.622	2.358	-5.3	15.162	15.991
8	-5.4	15.253	16.107	-5.2	15.366	16.149
9	-5.3	17.724	18.669	-4.9	31.011	31.739

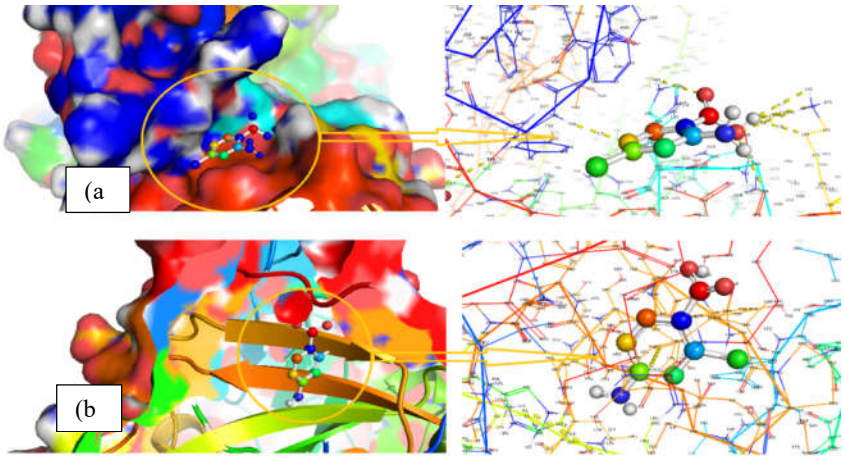

Figure 5. Docking diagram of the 6LU7 targed protein (a) 2A4ClBA and (b) 4A2ClBA.

As a result of theoretical calculations and experimental data, it was seen that the chemical and biological activity values of the 2A4ClBA molecule were higher than the 4A2ClBA molecule. The low ionization potential and high electron affinity of the 2A4ClBA molecule increased the chemical softness value. Due to its high chemical softness value, the inhibition effect of the 2A4ClBA molecule is thought to be greater than that of the 4A2ClBA molecule. It is noteworthy that molecular docking, dipole moments, static average polarizability and first hyperpolarizability values are consistent with these results. Urea takes place in the literature as a molecule with high polarizability value. In this study, the polarizability value of 2 benzoic acid derivatives was calculated as 3.3 times that of urea. Furthermore, the β values for 2a4ClBA and 4a2ClBA molecules are approximately 45 and 95 times higher than that of urea, respectively. This shows that cap molecules are very good candidates for nonlinear optical materials. According to molecular docking studied, 2A4ClBA and 4A2ClBA molecules showed binding affinities with Covid-19 protein in the range of 6.6-5.3 and 6.2-4.9 kcal/mol, respectively. This result suggests that the title molecules show activity against the 6LU7 protein.

ACKNOWLEDGMENTS

This work was supported by a grant (Project No: 3656-D2-13) from the Suleyman Demirel University Scientific Research fund.

REFERENCES

1. Alcolea Palafox, M.; Nunez, J.; Gıl, M. Theoretical quantum chemical study of benzoic acid: Geometrical parameters and vibrational wavenumbers. *Int. J. Quantum Chem*. **2002**, 89, 1-24.
2. Habib Rahuman, M.; Muthu, S.; Raajaraman, B.; Raja, M.; Umamahesvari, H. Investigations on 2-(4-cyanophenylamino) acetic acid by FT-IR,FT-Raman, NMR and UV-Vis spectroscopy, DFT(NBO, HOMO-LUMO, MEP and Fukui function) and molecular docking studies. *Heliyon* **2020**, 6, e04976.
3. Park, E.S.; Moon, W.S.; Song, M.J.; Kim, M.N.; Chung, K.H.; Yoon, J.S. Antimicrobial activityof phenol and benzoic acid derivatives. *Int. Biodeter. Biodegr.* **2001**, 47, 209-214.
4. Bao, Y.; Xu, R.; Zhao, H. 2-Amino-6-chlorobenzoic acid dissolved in numerous individual solvents: Equilibrium solubility, thermodynamic modeling, and mixing properties. *J. Chem. Eng*. **2020**, 65, 3252-3260.
5. Gamberini, M.C.; Mary, Y.S.; Mary, Y.S.; Krátky, M.; Vinsova, J.; Baraldi, C. Spectroscopic investigations, concentration dependent SERS, and molecular docking studies of a benzoic acid derivative. *Spectrochim. Acta - A: Mol. Biomol. Spectrosc.* **2021**, 248, 119265.
6. Stefaniu, A.; Pirvu, L.; Albu, B.; Pintilie, L. Molecular docking study on several benzoic acid derivatives against SARS-CoV-2. *Molecules* **2020**, 25, 5828.
7. Sabet, R.; Sisakht, M.; Emami, L.; Sabahi, Z. Comparison of COVID-19 virus main protease inhibition activities of phenolic acids by molecular docking. *Trends Pharmacol. Sci.* **2021**, 7, 117-126.
8. Cepas, V.; Soto, S.M. Relationship between virulence and resistance among gram-negative bacteria. *Antibiotics* **2020**, 9, 719.
9. Maurice, N.M.; Bedi, B.; Sadikot, R.T. Pseudomonas aeruginosa biofilms: Host response and clinical implications in lung infections, *Am. J. Respir. Cell Mol.* **2018**, 58, 428-439.
10. Hentzer, M.; Givskov, M. Pharmacological inhibition of quorum sensing for the treatment of chronic bacterial infections. *J. Clin. Investig*. **2003**, 112, 1300-1307.
11. Lynch, A.S.; Robertson, G.T. Bacterial and fungal biofilm infections. *Annual Rev. Med*. **2008**, 59, 415-428.

12. Dongari-Bagtzoglou, A. Pathogenesis of mucosal biofilm infections: challenges and progress, *Expert Rev. Anti-Infect. Ther.* **2008**, 6, 201-208.
13. Gupta, P.; Sarkar, S.; Das, B.; Bhattacharjee, S.; Tribedi, P. Biofilm, pathogenesis and prevention—a journey to break the wall: A review. *Arch. Microbiol.* **2016**, 198, 1-15.
14. Steward, P. Diffusion in biofilms. *ASM* **2003**, 185, 1485-1491.
15. Ulusoy, S.; Senkardes S.; Coskun, İ.; Bosgelmez-Tınaz, G.; Soulere, L.; Queneau, Y.; Kucukguzel, G. Quorum sensing inhibitor activities of celecoxib derivatives in *Pseudomonas aeruginosa*. *Lett. Drug. Des. Discov.* **2017**, 14, 613-618.
16. Önem, E.; Tüzün, B.; Akkoç, S. Anti-quorum sensing activity in *Pseudomonas aeruginosa* PA01 of benzimidazolium salts: electronic, spectral and structural investigations as theoretical approach. *J. Biomol. Struct*. **2021**, 1-12.
17. Kaya Kınaytürk, N.; Oturak, H. Identification of structural and spectral features of 2-amino 4-chlorobenzoic acid and 4-amino 2-chlorobenzoic acid: A comparative experimental and DFT study. *Acta Phys. Pol. A* **2016**, 130, 276-281.
18. Frisch M.J.; Trucks, G.W.; Schlegel, H.B.; Scuseria, G.E.; Robb, M.A.; Cheeseman, J.R.;Scalmani, G.; Barone, V.; Mennucci, B.; Petersson, G.A.; Nakatsuji, H.; Caricato, M.; Li, X., Hratchian, H.P.; Izmaylov, A.F.; Bloino, J.; Zheng, G.; Sonnenberg, J.L.; Hada, M.; Ehara, M.; Toyota, K.; Fukuda, R.; Hasegawa, J.; Ishida, M.; Nakajima, T.; Honda, Y.; Kitao, O.; Nakai, H.; Vreven, T.; Montgomery, J.A.; Peralta, J.E.; Ogliaro, F.; Bearpark, M.; Heyd, J.J.; Brothers, E.; Kudin, K.N.; Staroverov, V.N.; Kobayashi, R.; Normand, J.; Raghavachari, K.; Rendell, A.; Burant, J.C.; Iyengar, S.S.; Tomasi, J.; Cossi, M.; Rega, N; Millam, J.M.; Klene, M.; Knox, J.E.; Cross, J.B.; Bakken, V.; Adamo, C.; Jaramillo, J.; Gomperts, R.; Stratmann, R.E.; Yazyev, O.; Austin, A.J.; Cammi, R.; Pomelli, C.; Ochterski, J.W.; Martin, R.L.; Morokuma, K.; Zakrzewski, V.G.; Voth, G.A.; Salvador, P.; Dannenberg, J.J.; Dapprich, S.; Daniels, A.D.; Farkas, Ö.; Foresman, J.B.; Ortiz, J.V.; Cioslowski, J.; Fox, D.J. *Gaussian 09*, Gaussian, Inc.: Wallingford; **2003**.
19. Dennington, R.D.; Keith, T.A.; Millam, J.M. *Gauss Wiev 5.0*, Gaussian, Inc.: Wallingford; **2009**.
20. Lindstrom, W.; Morris, G.; Weber, C.; Huey, R. *Using AutoDock 4 for Virtual Screening*, **2008**.
21. Rabin, N.; Zheng, Y.; Opoku-Temeng, C.; Du, Y.; Bonsu, E.; Osintim, H. Biofilm formation mechanisms and targets for developing antibiofilm agents. *Future Med. Chem.* **2015**, 7 493-512.
22. Kaya Kınaytürk, N.; Kalaycı, T.; Tunalı, B. Experimental and computational investigations on the molecular structure, vibrational spectra, electronic properties, and molecular electrostatic potential analysis of phenylenediamine isomers. *Spectrosc. Lett.* **2021**, 54, 693-706.
23. Berrah, F.; Boursas, F.; Bouacida, S.; Ouannassi, F. Structural, spectroscopic and thermal characterizations combined with DFT calculationsand Hirshfeld analysis of a novel hydrogen-bonded complex: *p*-Phenylenediammonium dinitrate. *J. Mol. Struct*. **2020**, 1205, 127624.
24. Akman, F. A DFT study on molecular structure, MEP, HOMO–LUMO and spectroscopic analysis of thermoresponsive monomers used in micro/nanogel preparations. *J. Phys. Chem.* B **2021**, 15, 517-532.
25. Romani, D.; Noureddine, O.; Issaoui N.; Brandan, S.B. Properties and reactivities of niclosamide in different media, a potential antiviral to treatment of COVID-19 by using DFT calculations and molecular docking. *Biointerface Res. Appl. Chem.* **2020**, 10, 7295-7328.
26. Hagar, M.; Ahmed, H.A.; Aljohani, G.; Alhaddad, O. Investigation of some antiviral N-heterocycles as COVID 19 drug: Molecular docking and DFT calculations. *Int. J. Mol. Sci.* **2020**, 21, 3922.
27. Noureddine, O.; Issaoui, N.; Medimagh, M.; Dossary, O.A.; Marouani, H. Quantum chemical studies on molecular structure, AIM, ELF, RDG and antiviral activities of hybrid

hydroxychloroquine in the treatment of COVID-19: Molecular docking and DFT calculations. *J. King Saud Univ. Sci.* **2021**, 33, 101334.
28. Keçel-Gündüz, S.; Bıçak, B.; Çelik, S.; Akyüz, S.; Özel, A. Structural and spectroscopic investigation on antioxidant dipeptide, l-methionyl-l-serine: A combined experimental and DFT study. *J. Mol. Struct.* **2017**, 1137, 756-770.
29. Yadav, S.; Khare A.; Yadav, K.; Maurya, P.; Singh, A.; Kumar, A. Structure, vibrational analysis and chemical reactivity descriptors of 4-bromo-3-(methoxymethoxy) benzoic acid: A DFT study. *J. Sci Res.* **2022**, 14, 79-89.
30. Uğurlu, G. Study of the conformation analysis and electronic properties of 3, 5-dibromo-2-hydroxybenzoic acid molecule. *Caucasian J. Sci.* **2019**, 6, 51-63.
31. Kunduracıoğlu, A. 2–Amino–5–bromobenzoic acid: A Dft study for structural and molecular orbital analysis of tautomeric forms. *Open J. Nano* **2020**, 5, 17-22.
32. Anbarasan, R.; Enıya, P.; Sundar, J. Experimental and quantum chemical investigation on piperazinium hexachloro stannous trihydrate single crystal for second harmonic generation applications. *J. Electron. Mater.* **2019**, 48, 7686-7695.
33. Santhy, K.; Daniel Sweetlin, M; Muthu, S.; Kuruvilla, T.; Abraham, C. Structure, spectroscopic study and DFT calculations of 2,6 bis (tri fluro methyl) benzoic acid. *J. Mol. Struct.* **2019**, 1177, 401-417.
34. Kutlu, E.; Emen, F.; Kismali, G.; Kaya Kinaytürk, N.; Karaçolak, A.; Kiliç, D.; Ali, M.; Kutlu, H.; Demirdöğen, R. Synthesis and investigation of in vitro cytotoxic activities and thermal stability of novel pyridine derivative platinum(II) complexes vis a vis DFT studies, *Polyhedron* **2021**, 210, 115492.
35. Amin, A.; Ghosh, K.; Gayen, S.; Jha, T. Chemical-informatics approach to COVID-19 drug discovery: Monte Carlo based QSAR, virtual screening and molecular docking study of some in-house molecules as papain-like protease (PLpro) inhibitors. *J. Biomol. Struct.* **2021**, 39, 4764-4773.
36. Özdemir, M.; Köksoy, B.; Ceyhan, D.; Bulut, M.; Yalçın, B. In silico, 6LU7 protein inhibition using dihydroxy-3-phenyl coumarin derivatives for SARS-CoV-2. *J. Turk. Chem. Soc.* **2020**, 7, 691-712.
37. Marinho, E.M.; Neto, J.B.A.; Silva, J.; Silva, C.R.; Cavalcanti, B.C.; Marinho, E.S.; Junior, V.N. Virtual screening based on molecular docking of possible inhibitors of Covid-19 main protease, *Microb. Pathog.* **2020**, 148, 104365.
38. Muhammad, Z.; Farghaly, T.; Althagafi, I.; Hussain, S.; Zaki, M.; Harras, M. Synthesis of antimicrobial azoloazines and molecular docking for inhibiting COVID-19. *J. Heterocycl. Chem.* **2021**, 58, 1286-1301.
39. Tao, Q.; Du, J.; Li, X.; Zeng, J.; Tan, B.; Xu, J.; Lin, W.; Chen, X.L. Network pharmacology and molecular docking analysis on molecular targets and mechanisms of Huashi Baidu formula in the treatment of COVID-19. *Drug Dev. Ind. Pharm.* **2020**, 46, 1345-1353.